Environmental Science Nano

ROYAL SOCIETY OF CHEMISTRY

PAPER

View Article Online
View Journal | View Issue

Cite this: *Environ. Sci.: Nano*, 2021, **8**, 2718

Catalytic gold nanostars for SERS-based detection of mercury ions (Hg^{2+}) with inverse sensitivity†

Natasha Logan, ‡[a] Javier Lou-Franco,‡[a] Christopher Elliott[a] and Cuong Cao *[ab]

Gold nanostars (AuNSt) exhibit outstanding catalytic and plasmonic properties derived from their nano-size and shape. Their ability to mimic natural enzymes is exploited herein to oxidise 3,3′,5,5′-tetramethybenzidine (TMB) into an oxidised product (oxTMB), a highly Raman-active compound. AuNSt with different surface coatings including sodium citrate (NaCit), polyethylene glycol (PEG), oligoethylene glycol (OEG) and 11-mercaptoundecanoic acid (11-MUA) were prepared and characterised both as catalysts and Raman enhancers. AuNSt-PEG showed the best results as SERS substrates for oxTMB, therefore being chosen for the detection of mercury ions (Hg^{2+}). Hg is one of the most toxic elements known, and is a major environmental concern due to its adverse health effects. Hg is also known for forming amalgams with most metals, a property that is used in this study to alter the shape and size of AuNSt, thus limiting their Raman enhancement nature by amalgamating their sharp tips which are responsible for most SERS 'hot spots'. As a result, the Raman peak of oxTMB at 1190 cm^{-1} shows an inverse linear dependence with increasing Hg^{2+} ion concentration. This approach achieved a limit of detection of 0.2 ppb in seawater (certified reference materials, CRM), and a linear response between 0.1 and 1000 ppb. Thus, this ground-breaking technique could contribute to the protection of water systems, aquaculture and human health, whilst providing a biosensing platform for numerous applications in the future.

Received 15th June 2021,
Accepted 17th August 2021

DOI: 10.1039/d1en00548k

rsc.li/es-nano

Environmental significance

Mercury (Hg^{2+}) pollution of seawater has been identified as a major and global environmental concern due its high toxicity. It can bioaccumulate in marine life, and eventually pose a threat to human health through seafood consumption. The enzyme-mimicking and Raman enhancement properties of gold nanostars (AuNSt) are exploited to detect trace levels of Hg^{2+} ions in certified seawater samples, with a detection limit of 0.2 ppb. It is demonstrated that in the presence of Hg^{2+} ions, amalgamation with the AuNSt negatively affects their potential as Raman enhancers, by altering their unique morphology. Thus, providing a sensitive and highly specific mechanism for Hg^{2+} ion detection, which could protect environmental samples (*e.g.*, food, water, soil) in the future.

1. Introduction

Since around 5000 BC, the naturally occurring ore of mercury (Hg) (cinnabar or vermilion) has been used in the manufacturing of red ink and paint for artwork, decoration and tattoo dyes.[1,2] Due to its low melting point, Hg is the only liquid metal at room temperature.[3] This unique property allows Hg to form amalgams with almost all metals, except iron (Fe) and platinum (Pt).[4] Hg-amalgams have had numerous uses in society, *e.g.* gold (Au) extraction,[1] production of industrial chemicals such as hydrogen peroxide (H_2O_2) and chlorine[5] and the "silver (Ag)-amalgam" tooth filling in dentistry.[1]

While Hg has been shown to be very useful in the intended applications, contamination of Hg in the environment and in foods poses substantial environmental and health risks. Therefore, sensitive detection of Hg is of crucial importance for food and environmental monitoring and protection. Hg can be detected by conventional methods such as cold-vapor atomic fluorescence spectrometry (CV-AFS), inductively coupled plasma-mass spectrometry (ICP-MS), and X-ray absorption spectroscopy (XAS). Today within nanoscience research, Hg amalgamation with noble metal nanomaterials (*i.e.*, Ag, Au, or Pt) has encouraged the development of plasmonic and catalytic approaches to improve Hg detection with regards to sensitivity, ease of use, and cost-effectiveness. Advantages of the enhanced catalytic activity observed with Au–Hg,[6] Ag–Hg,[7] and Pt–Au–Hg (ref. 8)

[a] *Institute for Global Food Security, School of Biological Sciences, Queen's University of Belfast, 19 Chlorine Gardens, Belfast, BT9 5DL, UK. E-mail: c.cao@qub.ac.uk*
[b] *Material and Advanced Technologies for Healthcare, Queen's University of Belfast, 18-30 Malone Road, Belfast, BT9 5BN, UK*

† Electronic supplementary information (ESI) available. See DOI: 10.1039/d1en00548k

‡ These authors contributed equally to this work.

alloys have been exploited for the development of colorimetric,[9] fluorescent,[10] and SERS-based detection of Hg^{2+} (ref. 11) even in harsh matrices, *e.g.* seawater.[12] Several studies have also revealed that the amalgamation with Hg^{2+} could transform the morphology of anisotropic nanomaterials and this phenomenon has been exploited for Hg^{2+} detection. Rex *et al.* presented the interactions between Hg and Au which resulted in wavelength changes to the absorption spectra of Au-nanorods.[13] Reduced aspect ratios and subsequent surface plasmon resonance (SPR) blue-shifts could therefore be exploited to determine subsequent Hg concentrations. Additionally, Senapati *et al.* reported that Au-popcorn shaped NPs protected with tryptophan,[14] a Raman-active tag suffered from reduced SERS as a result of tryptophan release and changes to the morphology of the popcorn-shaped AuNPs after Au–Hg amalgamation.

In this study, we report on a novel, label-free approach that combines the excellent catalytic and SERS activities of AuNSt for the detection of Hg^{2+} ions in seawater. The unique morphology of AuNSts, *i.e.* their sharp tips, could produce phenomenal Raman enhancement,[15–17] and therefore they have also been exploited for the design of SERS-sensors for Hg^{2+} detection.[18,19] Unlike previously reported research, the presented mechanism involves the catalytic activity of AuNSt for the oxidation of 3,3′,5,5′-tetramethybenzidine (TMB) in the presence of H_2O_2 to produce oxidised TMB (oxTMB), a highly Raman active product.[20–22] We observed that in the presence of Hg^{2+} ions, the Au–Hg amalgamation could even enhance the catalysed oxidation reaction as evident by the strong blue coloured oxTMB product. As stated, oxTMB is also a Raman-active residue, therefore one would reasonably expect a strong Raman signal owing to the SERS effect of AuNSts. However, experimental analysis showed an opposed reduction in Raman intensity from the reporter oxTMB in the presence of AuNSt and Hg^{2+} ions. Electron microscopy and elemental analysis further revealed that the presence of Hg^{2+} destructively truncated the sharp tips of the AuNSt changing their size, shape, and elemental composition. As a result, the amalgamated Au–Hg nanostructures were not effective in the SERS-sensing process under the experimental conditions. Thus, the mechanism provides a platform with inverse sensitivity for Hg^{2+} detection, whereby the catalysed oxTMB signal measured by SERS is inversely proportional to the Hg^{2+} ion concentration. Overall, the developed SERS-sensor can allow the sensitive detection of Hg^{2+} in seawater and has the potential to be incorporated into different biosensing applications, including medical diagnostics, food analysis and environmental protection.

2. Materials and methods

2.1 Chemicals and reagents

Sodium citrate tribasic dehydrate ($HOC(COONa)(CH_2COONa)_2{\cdot}aq$), gold(III) chloride trihydrate ($HAuCl_4{\cdot}3H_2O$, 99.9%), mercury(II) perchlorate hydrate ($Hg(ClO_4)_2{\cdot}xH_2O$, 99.998%), *O*-(3-carboxypropyl)-*O*′-[2-(3-mercaptopropionylamino)ethyl]-polyethylene glycol (molecular weight = 5000, $SHCH_2CH_2[OCH_2CH_2]_{110}OCH_2CH_2COOH$), 11-mercaptoundecanoic acid, *O*-(2-carboxyethyl)-*O*′-(2-mercaptoethyl)heptaethylene glycol (molecular weight = 458.56, $SHCH_2CH_2[OCH_2CH_2]_7OCH_2CH_2COOH$), sodium chloride (NaCl), hydrochloric acid (HCl), sodium hydroxide (NaOH), rhodamine 6G, 3,3′,5,5′-tetramethybenzidine (TMB), hydrogen peroxide (H_2O_2), nitric acid (HNO_3), acetic acid (CH_3COOH), sodium acetate (CH_3COONa), silver nitrate ($AgNO_3$), ascorbic acid (L-AA) and all metallic ions were purchased from Sigma Aldrich (UK). Syringe filters (0.22 μm) were purchased from Merck Millipore (Germany). A coastal seawater Hg^{2+} certified reference material (CRM) was purchased from LGC Standards (UK).

2.2 Analysis instrumentation

Ultraviolet-visible spectroscopy (UV-vis) measurements were performed using a Cary 60 spectrophotometer (Agilent Technologies, USA). SERS measurements were carried out using a DXR2 Raman microscope operated with an excitation laser light at 785 nm (Thermo Fisher Scientific, UK). Fourier-transform infrared (FTIR) spectroscopy measurements were conducted on a Nicolet iS5 FTIR spectrometer (Thermo Fisher Scientific, UK). Transmission electron microscopy (TEM) measurements were performed using a Joel JEM 1400 Plus model, operated at 200 kV (Thermo Fisher, Scientific, UK). High resolution TEM, scanning transmission electron microscopy (STEM), and high angle annular dark field (HAADF) analyses were conducted using a Talos F200 operated at 200 kV (Thermo Fisher Scientific, UK). Elemental analysis was obtained by energy-dispersive X-ray spectroscopy (EDS) equipped with the TEM system.

2.3 Synthesis of Au nanostar (AuNSt) and stabilisation with different surface coatings

Gold nanoparticles (AuNP) were synthesised using the sodium citrate reduction of $HAuCl_4$ as described previously,[23] and used as Au seeds for the AuNSt synthesis. Briefly, 1 mM of $HAuCl_4$ was dissolved in 100 mL of deionised water (dH_2O) and heated until rapidly boiling. Upon reflux, 10 mL of 1% sodium citrate (NaCit) was quickly added under vigorous stirring. The solution was removed from the heat upon a colour change from yellow to wine-red. Subsequently, AuNSt (98 ± 19.18 nm) were synthesised following a previous method with minor adjustments.[24] Briefly, 25 μL of $HAuCl_4$ (100 mM) and 5 μL of HCl (2 M) were added to 10 mL of dH_2O, under continuous stirring. Au seeds were subsequently added (75 μL), followed by 100 μL of $AgNO_3$ (3 mM) and 50 μL of L-AA (100 mM). After a few seconds the AuNSt-mixture changes colour from clear to blue-green (Fig. SI.1†).

Stabilisation of the prepared AuNSt was achieved by incubating overnight with a final concentration of 1 mM of NaCit, under minor stirring conditions at room temperature. Various functionalisation approaches were alternatively used, leading to 11-mercaptoundecanoic acid (11-MUA)-coated, polyethylene glycol (PEG)-coated or oligoethylene glycol

(OEG)-coated AuNSt. The former was conducted by replacing the citrate molecules with 11-MUA at a concentration of 100 μM in an ethanol : water 1 : 1 solution (v/v), under minor stirring conditions overnight at room temperature. Functionalisation of the AuNSt with PEG was conducted as reported previously with minor adjustments.[25] Immediately after synthesis, 0.8 μM of PEG was added to the AuNSt solution and stirred continuously for 15 min at room temperature. OEG-capped AuNSt were obtained after adding 500 μM of OEG to the AuNSt solution and stirred overnight at room temperature. Finally, the particles were centrifuged at 10 °C, 1200 rcf for 25 min to remove unbound 11-MUA/PEG/OEG and re-suspended in dH_2O (stored at 4 °C).

2.4 SERS-based detection of Hg^{2+} using AuNSt-PEG as nanozymes for TMB oxidation

Prior to analysis, a stock solution of Hg^{2+} was prepared at 20 000 ppm in 0.02 M HNO_3 (stored at 4 °C). In a typical experiment, Hg^{2+} concentrations ranging from 0–100 ppm were prepared in dH_2O and transferred to a 96-well ELISA plate (100 μL). The AuNSt-PEG conjugate was subsequently added (50 μL, as-prepared), followed by 1.25 mM TMB and 6% H_2O_2 (150 μL), and incubated for 20 min at room temperature. A coastal seawater certified reference material (CRM) was spiked with Hg^{2+} concentrations ranging from 0–100 ppm and the previous assay was repeated. Prior to measurement, the Raman microscope was focused by monitoring the catalytic activity of the blank/zero solution (PEG-AuNSt and 1.25 mM TMB with 6% H_2O_2 without Hg^{2+}) and using the 'Autofocus' function available with OMNIC™ series software (Thermo Fisher Scientific, UK) to acquire maximum Raman intensity. Once focused, the same conditions were applied throughout and all samples were measured in solution.

3. Results and discussion

3.1 Characterisation of AuNSt as catalysts and Raman enhancers

Aggregation of colloidal gold nanoparticles is subjected to short-range thermodynamic interactions that allow for particle – particle attachment to occur, whereas Brownian diffusion controls long-range forces, causing collisions between nanoparticles (NPs).[26] If NPs were not stabilised, this would result in the formation of larger clusters no longer

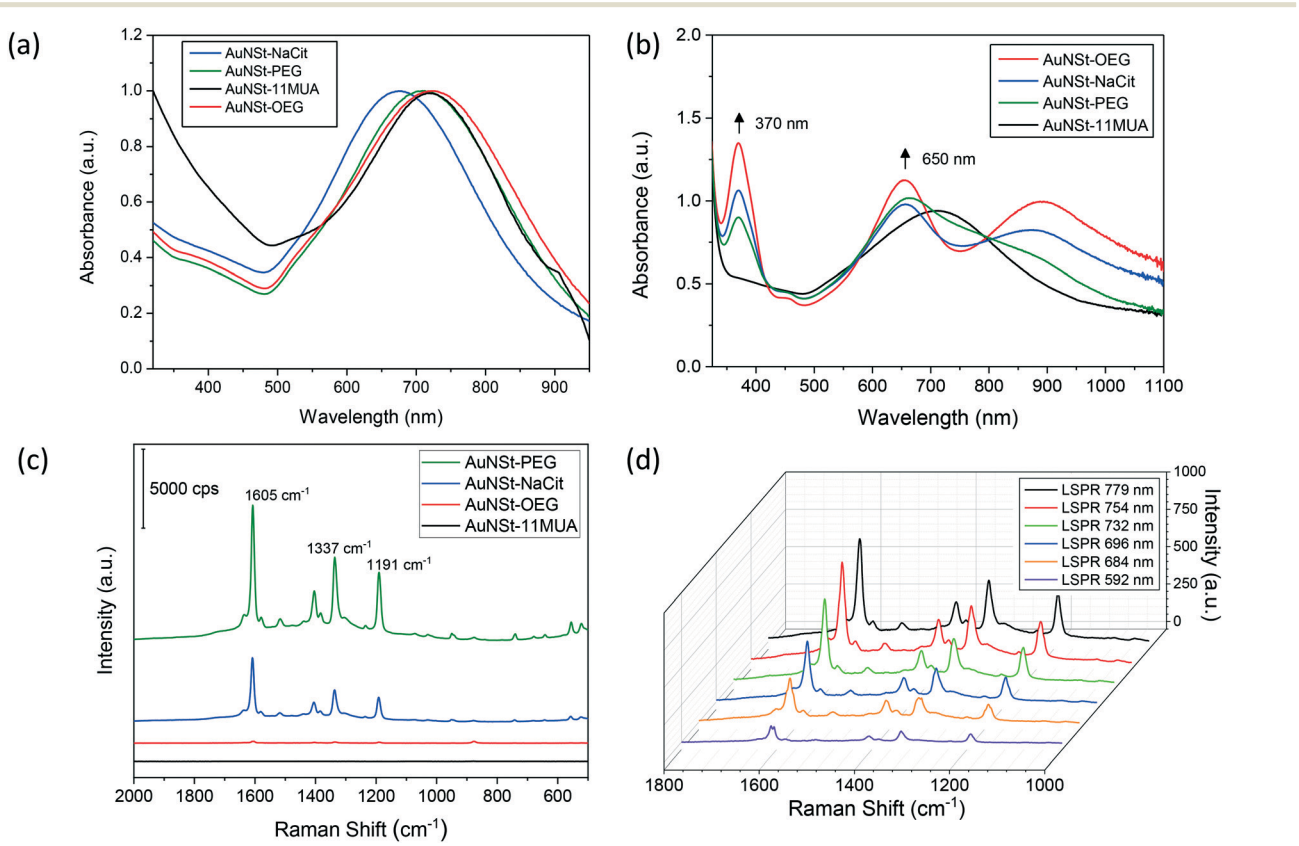

Fig. 1 Enzymatic and spectroscopic characterisation of AuNSt. (a) Absorption spectra of AuNSt functionalised with different coating molecules. (b) UV-vis spectroscopy analysis of TMB oxidation. 200 pM AuNSt coated with different molecules were mixed with 0.1 mM TMB in an aqueous solution containing 6% H_2O_2. The spectra were collected after 20 min of reaction. (c) oxTMB generated in (b) was measured by Raman spectroscopy. Raman measurements were performed using a laser power of 10 mW, wavelength source 785 nm, 10 exposures with an integration time of 5 s and a 10x objective lens. (d) AuNSt-NaCit with different plasmonic properties were analysed by Raman spectroscopy to detect the presence of oxTMB. A laser power of 2 mW was used, keeping the rest of conditions unvaried.

exhibiting the many properties derived from the nanoscale. The most common approach to avoid this consists of adsorbing polymers and polyelectrolytes to provide electrostatic repulsions that prevent NP aggregation. Therefore, AuNSt stabilised with different coating molecules were produced to be used as nanozymes and Raman enhancers for a Hg detection system. The synthesis and functionalisation of AuNSt was characterised using UV-vis spectroscopy (Fig. 1a). AuNSt stabilised with NaCit showed a localized surface plasmon resonance (LSPR) at 670 nm, whereas the resonance red-shifts if the stabilising agent is changed, resulting in 712 nm, 717 nm and 723 nm for AuNSt stabilised with PEG, 11-MUA and OEG, respectively.

It has been documented that coating layers and surface chemistry can lead to unexpected positive or negative effects on the catalytic activities of nanozymes.[27] Therefore, the capability of the synthesised AuNSt to act as nanozymes for the oxidation of TMB was also analysed by UV-vis (Fig. 1b). The emergence of two peaks enabled the monitoring of the catalytic reaction. The peak at 370 nm was found to be characteristic of the radical cation (TMB^+), whereas the peak at 650 nm represented a blue charge transfer complex (CTC), both of which coexisted during the TMB oxidation process.[22] Overall, AuNSt have previously displayed decent catalytic efficiency values for peroxidase-like activity when compared with different shaped AuNPs or even biological enzymes, being outperformed only by smaller Au nanospheres.[27] As for their surface nature, as shown in Fig. 1b, AuNSt-OEG exhibited the highest catalytic activity among the samples analysed, followed by AuNSt-NaCit and AuNSt-PEG. On the other hand, AuNSt-11-MUA did not show any sign of TMB oxidation. This may be due to the three-dimensional organisation of the polymeric chains used as stabilisers, which in the case of 11-MUA (an aliphatic chain with a polar head) would arrange densely packed onto the AuNSt surface due to hydrophobic interactions. This would impede the substrate to reach the catalytically active gold surface, whereas this would not be observed when hydrophilic polymers such as PEG/OEG are used as stabilisers.[28] However, this approach to detect the oxidation of TMB lacks sensitivity, especially when applied for real diagnostic applications where low levels of target analyte are to be detected (Fig. SI.2†). Thus, this explains why AuNSt were not only used as nanozymes, but also as Raman enhancers in this study. In addition, TMB is a substrate involved in peroxidase-mediated reactions and its product (oxTMB) is also highly Raman active. Therefore, by incorporating a peroxidase substrate and a Raman active product into the mechanism one can hypothesise that both the sensitivity and specificity of the approach can be improved.

The samples containing oxTMB in the vicinity of the AuNSt were analysed with the Raman microscope to develop a SERS sensor, due to the Raman active nature of oxTMB and the capability of anisotropic NPs to enhance Raman signals.[17,29] Three main Raman bands corresponding to oxTMB could be observed at 1608 cm^{-1}, 1336 cm^{-1} and 1190 cm^{-1} (Fig. 1c), which could be attributed to ring stretching and C–H bending, inter-ring C–C stretching and CH_3 bending, respectively.[22] These provided evidence that a blue CTC had occurred, due to the oxidation of TMB.[20] In addition, another Raman band at 1401 cm^{-1} was observed in the fingerprint spectra of oxTMB from the stretching vibration of N=N, as a result of azo compound or unoxidized TMB, which was also enhanced by the presence of AuNSt.[21] However, it was interesting to note that only AuNSt-PEG and AuNSt-NaCit could generate such Raman signals, whilst in the case of AuNSt-11-MUA there was no TMB oxidation at all (and therefore no Raman signal was generated). AuNSt-OEG oxidised TMB but failed to act as good Raman enhancers (peaks under 100 a.u.). We also observed a similar result when rhodamine-6-G (a typical Raman reporter) was used instead of the oxTMB product (Fig. SI.3†). Therefore, we speculated that the strong SERS signals were because of the hydrophilicity and the molecular conformation of the coating moieties that facilitate or prevent the analytes (*i.e.* oxTMB, rhodamine-6-G) from penetrating into the SERS hot spots. In fact, in terms of water solubility, AuNSt-11-MUA is the most hydrophobic SERS substrate due to the alkane backbone of 11-MUA, whilst AuNSt-NaCit is the most hydrophilic. Due to increased ethylene glycol ($–O–CH_2–CH_2–$) units, the PEG molecule in this study provides more O atoms which act as template for water nucleation than that of the OEG molecule (110 *versus* 7 ethylene glycol units, respectively). Therefore, AuNSt-PEG is more hydrophilic than AuNSt-OEG albeit both exhibiting amphiphilic behaviour. Based on this speculation, oxTMB or rhodamine-6-G will have easier access to the surface of the aqueous AuNSt-PEG, and therefore will result in improved SERS signals than those obtained with the AuNSt-OEG. Muehlethaler *et al.* also observed that it is very challenging to obtain SERS signals if dyes or target molecules do not provide the necessary adsorption or proximity to SERS substrates.[30] These interesting findings led to the selection of AuNSt-PEG as the material of choice for further studies, as they effectively oxidised TMB and provided essential Raman enhancement. However, all nanomaterials mentioned in this study also have the potential to be used for different biosensing applications (*e.g.*, medical diagnostics, food analysis, environmental protection) and within numerous research fields. Moreover, characterisation to support proper particle stabilisation was determined by analysing the UV-vis spectrum of AuNSt-PEG in a high electrolyte matrix (3.5% NaCl or seawater conditions) (Fig. SI.4†) and through the identification of PEG molecules on the surface of the AuNSt *via* FTIR spectroscopy (Fig. SI.5†).

Following previous studies,[31] the analytical enhancement factor (AEF) observed for unmodified AuNSt (*i.e.* stabilised with NaCit) was 2.1×10^5 (Fig. SI.6†). Therefore, in this study SERS could be enhanced by 5 orders of magnitude in respect to Raman scattering alone, enhancements similar to those reported previously.[17,32] However, the capability of AuNSt to enhance the Raman signal was not only dependant on the nature of any surface modification, but also on its LSPR

wavelength. By varying the amount of gold seeds used during the synthesis (refer to section 2.3), the size of the resulting AuNSt was tuned, leading to a range of LSPR values. AuNSt stabilised by NaCit having various LSPR modes were tested as Raman enhancers after generating similar concentrations of oxTMB (Fig. 1d). The results displayed that the AuNSt whose LSPR wavelength was closer to the laser excitation wavelength led to improved enhancement, whilst keeping identical measurement conditions and parameters consistent for all samples. The explanation for this observation lies in the LSPR of the AuNSt being generated by the conduction electrons oscillating at a certain frequency at the surface of the NP. Thus, the amplitude of these oscillations was increased when an external light source was applied to them with the plasmonic frequency, resulting in increased electromagnetic field enhancements in the vicinity of the AuNSt. Moreover, previous studies on single AuNSt have shown that these electromagnetic hot spots are mainly located at their tips,[33] whose length and sharpness are correlated to their LSPR.[24] Overall, this explains why the higher Raman enhancement is observed for AuNSt when their LSPR wavelength approaches 785 nm (Fig. SI.7†). Considering all the above, AuNSt-PEG with LSPR at 781 nm were selected for developing the mercury ion (Hg^{2+}) sensor, as they have demonstrated two fundamental qualities: good catalytic properties for the oxidation of TMB and excellent Raman enhancement properties. In addition to these properties held by AuNSt-PEG, Hg^{2+} also has the unique ability to amalgamate with Au thus, allowing for the design of a sensitive Hg^{2+} ion sensor with high specificity.

3.2 Characterisation of AuNSt-PEG in the absence and presence of Hg^{2+} ions

HRTEM was conducted to characterise the morphology of AuNSt-PEG in the absence (Fig. 2a) and presence of 100 ppm

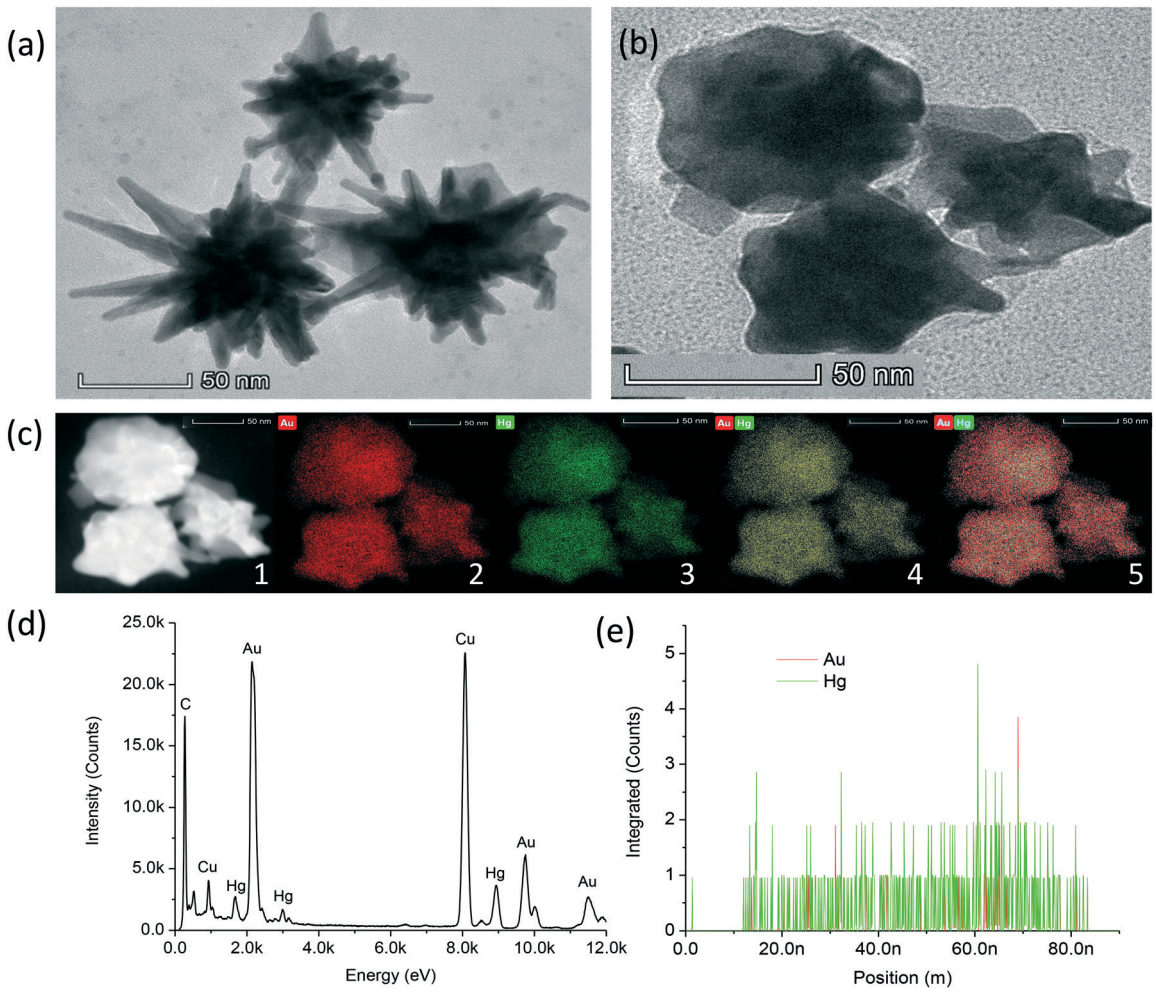

Fig. 2 Characterisation of AuNSt-PEG in the presence of Hg^{2+} (100 ppm). (a) High resolution transmission electron microscopy (HRTEM) in the absence and (b) presence of 100 ppm Hg^{2+}. (c) Scanning transmission electron microscopy (STEM) and elemental analysis. (1) High-angle annular dark-field imaging (HAADF-STEM) of the sample presented in (b). Elemental analysis of (2) Au (3) Hg^{2+} (4) Au and Hg^{2+} (5) Au and Hg^{2+} (post-filtered image). (d) Energy-dispersive X-ray spectra (EDS) of the particle presented in (b). (e) Positional spectra from EDS of Au and Hg^{2+} within one particle illustrated in (b).

Hg^{2+} (Fig. 2b). The results confirmed the shape of the particles after synthesis and demonstrated how the morphology of the AuNSt-PEG changed in the presence of Hg^{2+} ions. HRTEM confirmed that the particles began as star-shaped and eventually resulted in spherical-like, or ill-defined shaped particles after Au–Hg amalgamation. To rule out any changes to the AuNSt-PEG morphology caused by a lack of particle stability or aggregation, HRTEM images of AuNSt-PEG in the absence and presence of 100 ppm Hg^{2+} ions (Fig. SI.8a and b,† respectively) and UV-vis spectroscopy were exploited to confirm the stability of AuNSt-PEG in the presence of different Hg^{2+} concentrations (1–10^2 ppm) (Fig. SI.8c†). Additionally, kinetic analysis was utilised to monitor the stability at the peak absorbance of 781 nm over a 30 min incubation in the presence of 10 ppm Hg^{2+} ions (Fig. SI.8d†). From the results, we could confirm that changes to the shape of the AuNSt-PEG were not due to particle aggregation, and therefore we can hypothesise that Au–Hg amalgamation is the cause of the morphology changes witnessed using HRTEM. It was also important to note the timing difference in sample preparation between UV-vis (Fig. SI.8c:† 10 min) and HRTEM (Fig. 2b: 24–48 h). Thus, the morphology transformation due to Au–Hg amalgamation could be fully observed using HRTEM. From the HRTEM images, 50 particles were analysed using ImageJ software and the size of the AuNSt-PEG in the absence and presence of Hg^{2+} was estimated to be 116 nm ± 18.6 nm (from tip-to-tip), and 65 nm ± 17.5 nm (after truncation), respectively (Fig. SI.9†). Thus, by HRTEM it could be confirmed that Hg^{2+} played a significant role in destroying the branches of the AuNSt, which resulted in a substantial decrease in particle size.

The DLS results for AuNSt-NaCit alone, AuNSt-PEG alone and AuNSt-PEG with 10 ppm Hg^{2+} were 98 nm, 119 nm and 102 nm, respectively (Fig. SI.10a†). The increased size between NaCit and PEG was solely due to the large PEG-thiol molecule (MW = 5000), which was found to displace NaCit and coil around the surface of the AuNSt forming a layer.[34] As expected, the size of the AuNSt-PEG decreased in the presence of Hg^{2+} as the sharp tips of the AuNSt-PEG became truncated after Au–Hg amalgamation. Zetasizer analysis revealed the charge for the AuNSt-NaCit, AuNSt-PEG and AuNSt-PEG in the presence of Hg^{2+} as −47 mV, −20 mV and −17 mV, respectively (Fig. SI.10b†). PEG-functionalisation and the addition of Hg^{2+} both resulted in the AuNSt becoming more neutrally charged, which is attributed to the positive charge held by the amino groups present in the chemical structure of PEG and the two positive groups held by Hg^{2+} ions.[11]

STEM imaging (Fig. 2c), HAADF-STEM (Fig. 2c, inset: 1), elemental mapping (Fig. 2c, inset: 2–5), EDS (Fig. 2d) and positional analysis spectra (Fig. 2e) were conducted to confirm the sensing mechanism was due to the amalgamation of AuNSt with Hg^{2+} ions. From the results, it could be confirmed that Hg had amalgamated with the AuNSt. The results from the elemental mapping performed using HAADF-STEM imaging revealed the presence of a uniform Hg coating around the AuNSt-PEG. The displacement of PEG on the surface with Hg^{2+} could be attributed to the reduction of Hg^{2+} to Hg^0, which resulted in Au–Hg amalgam. The elemental mapping clearly displayed the distribution of Au (Fig. 2c: inset 2, red), Hg (Fig. 2c: inset 3, green) and both elements together (Fig. 2c: inset 4–5, yellow or red and green, respectively), surrounding the AuNSt-PEG which confirmed successful Au–Hg amalgamation. Additionally, the EDS (Fig. 2d) clearly indicated the presence of both Au and Hg within the same particle (presented in Fig. 2b). Furthermore, the positional analysis spectra (Fig. 2e), confirmed that within one particle (presented in Fig. 2b) the presence of Hg was much greater than Au. This could be attributed to Hg displacing the Au from the particle surface during amalgamation. Overall, these results strongly support that the sensing mechanism was due to the damaging effect that Hg^{2+} had on the sharp tips of the AuNSt, which was initiated by Au–Hg amalgamation.

3.3 Catalytic activity and Raman enhancement of AuNSt-PEG in the presence of Hg^{2+} ions

Whilst previous studies have reported that Au–Hg amalgamation enhanced the catalytic performance of spherical AuNPs,[35] the peroxidase-like activity and Raman enhancement of the AuNSt in the presence of Hg^{2+} ions was yet to be explored. Kinetic analysis was conducted using Raman spectroscopy to monitor the oxidation of 1.25 mM TMB with 6% H_2O_2 by AuNSt-PEG in the absence and presence of Hg^{2+} ions. The Raman signal which could be observed in the absence of Hg^{2+} ions was generated by the formation of oxTMB by AuNSt-PEG in the presence of 1.25 mM TMB/6% H_2O_2 (Fig. 3a, red line), as no signal was generated by AuNSt-PEG alone (Fig. 3a, black line). However, in the presence of 10 ppm or 100 ppm Hg^{2+} (Fig. 3a, blue and cyan line, respectively) the intensity of the SERS spectra from oxTMB was significantly and proportionally reduced with the addition of Hg^{2+}. To further confirm this phenomenon, the catalytic reaction in the absence and presence of 100 ppm Hg^{2+} was analysed by kinetic Raman spectroscopy over 30 min. The results clearly indicate the production of oxTMB over time (Fig. 3b) however, in the presence of Hg^{2+} ions, the SERS signal of oxTMB is gradually diminished (Fig. 3c). As mentioned previously, the catalytic activity of spherical particles can be negatively influenced by increasing particle size or particle aggregation, due to a reduction in surface area-to-volume ratio.[12] However, the results provided in Fig. SI.6† can confirm that the decline in catalytic activity is not caused by aggregation. In fact, UV-vis spectroscopy and kinetic analysis of the AuNSt-PEG with TMB/6% H_2O_2 in the absence and presence of Hg^{2+} ions, further confirmed that the catalysis reaction of TMB substrate could be enhanced by Au–Hg amalgamation and was not adversely affected by the presence of Hg^{2+} (Fig. SI.11†). Therefore, the decline in catalytic activity witnessed by SERS is due to the disruption of the

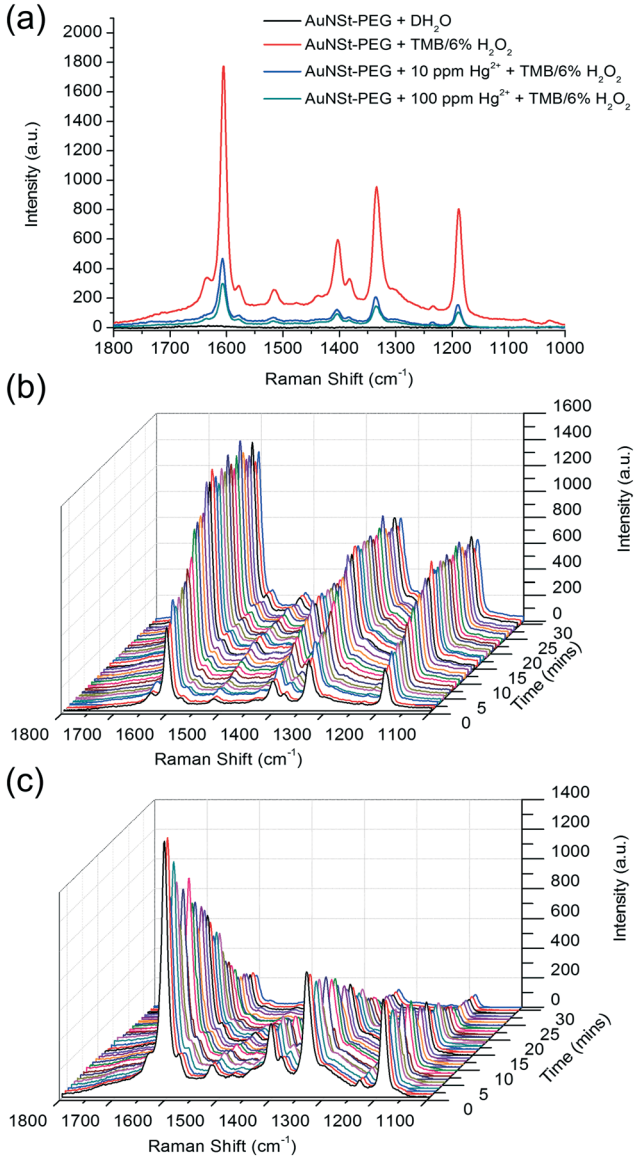

Fig. 3 Kinetic analysis for AuNSt-PEG in the absence and presence of Hg^{2+} ions confirming increased and decreased SERS intensity, respectively. All measurements are in the presence of 1.25 mM TMB and 6% H_2O_2. (a) Full Raman spectrum of the oxTMB SERS signal catalysed by AuNSt-PEG (red line) and the reduction in SERS intensity with Hg^{2+} at 10 ppm and 100 ppm (blue and cyan line, respectively). Kinetic Raman spectroscopy analysis of the catalytic product (oxTMB) produced over a 30 min incubation by AuNSt-PEG in the (b) absence and (c) presence of 100 ppm Hg^{2+}. Raman measurements were performed using a laser power of 20 mW, wavelength source 785 nm, 10 exposures with an integration time of 5 s and a 10× objective lens.

sharp tips of the AuNSt after Au–Hg amalgamation, thus the number of available 'hot spots' for SERS enhancement was reduced. Overall, both UV-vis and SERS analysis can confirm the catalysis reaction of chromogenic substrate (TMB) into a blue coloured product (oxTMB) in the presence of AuNSt-PEG and Hg^{2+}. However, the SERS signal from oxTMB could also detect changes to the AuNSt-PEG morphology and as a result the SERS intensity was reduced.

3.4 SERS sensing principle for Hg^{2+} detection

As illustrated in Scheme 1, the detection mechanism for Hg^{2+} is based on both the catalytic activity of AuNSt-PEG and their role as Raman enhancers. It was evident that AuNSt-PEG can catalyse for the oxidisation of TMB substrate to generate a highly Raman active product (oxTMB) (Fig. SI.1†) that can be measured by taking advantage of the AuNSt as a SERS substrate (Scheme 1a). The morphology of the AuNSt results in excellent enhancement of the electromagnetic field due to the sharp tips of the particles. The addition of Hg^{2+} ions does not interfere with the catalytic activity of AuNSt for the oxidation of TMB, however the tips of the AuNSt are disrupted because of the formation of Au–Hg amalgam (Scheme 1b). Without their sharp tips, the AuNSt-PEG was found to no longer provide the 'hot spots' required for Raman enhancement. Therefore, the Raman signal of oxTMB will decrease with increasing concentrations of Hg^{2+} ions, thus providing a mechanism for the detection of Hg^{2+} ions with inverse sensitivity.

3.5 Sensitivity of the SERS-based detection of Hg^{2+} ions using the catalytic gold nanostars

Assay parameters, *i.e.* AuNSt-PEG concentration, oxTMB SERS peak, and incubation time required further optimisation to ensure that the optimum conditions were applied for Hg^{2+} detection. The kinetic analysis results over 30 min (Fig. SI.12a†) confirmed that the SERS band at 1190 cm^{-1} gave a linear response against Hg^{2+} concentration after 20 min (Fig. SI.12b†). Therefore, for maximum SERS enhancement a AuNSt-PEG concentration of OD_{781nm} = 3.0, oxTMB peak at 1190 cm^{-1} and an incubation time of 20 min were chosen as the optimum assay parameters. Analysis of the full SERS spectra (Fig. 4a) and the oxTMB band at 1190 cm^{-1} (Fig. 4b) provides clear evidence that increasing the concentration of Hg^{2+} ions led to a decreased SERS signal coming from oxTMB, therefore inverse sensitivity could be observed. These results are attributed to Au–Hg amalgamation and the truncation of the sharp branches of the AuNSt-PEG in the presence of Hg^{2+} ions, confirmed earlier by HRTEM. Although the resulted amalgamated nanostructures retained their peroxidase-like activity which effectively catalysed the conversion of TMB to oxTMB, their Raman enhancement property was significantly reduced. As the branches on the AuNSt surface are crucial to provide SERS enhancement, the reduction of 'hot spot' centers could be exploited for the detection of Hg^{2+}. The calibration curve which demonstrates the oxTMB peak at 1190 cm^{-1} against Hg^{2+} concentration provided a working range from 0.1 ppb to 10^5 ppb (Fig. 4c). Additionally, the linear fitting was within the range of 0.1 ppb to 10^3 ppb Hg^{2+} ions (R^2 = 0.987) in a dH_2O matrix, under optimised conditions (Fig. 4d). The Limit of Detection (LOD) was calculated based on a combination of the International Union of Pure and Applied Chemistry (IUPAC) definition (3S/M) and the calibration curve procedure as LOD concentration (x) = y–c/m, whereby y is the standard deviation

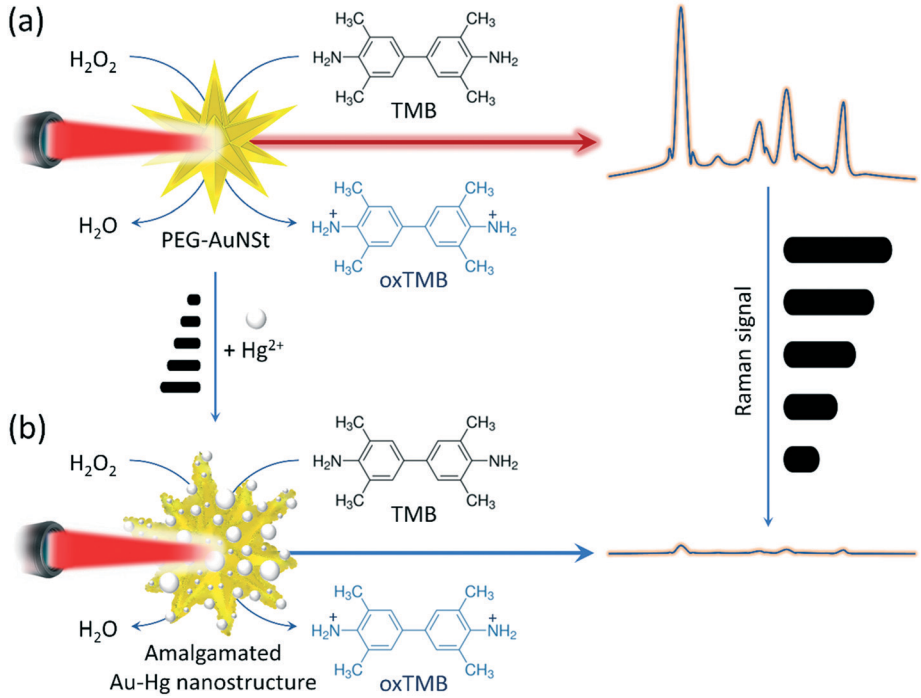

Scheme 1 Working principle of the SERS-sensing approach using catalytic AuNSt for the detection of Hg^{2+} ions. (a) In the presence of AuNSt-PEG, 1.25 mM TMB and 6% H_2O_2, TMB is catalysed into a highly Raman active product (oxTMB) that allows a strong SERS intensity to be measured using the PEG-AuNSt. (b) The catalytic activity of AuNSt-PEG remains in the presence of Hg^{2+} ions. However, decreased SERS intensity is observed when the morphology of the AuNSt-PEG is altered as a result of Au–Hg amalgamation.

of three measurements of the blank and c and m are the intercept and the gradient of the calibration curve, respectively. Due to the linear range (0.1–10^3 ppb) falling within the calibration range, the lowest concentration was very close to the saturation point of the assay. Therefore, the lowest detectable limit of the SERS-sensor which could be accurately distinguished from the background signal was calculated as 0.249 ppb Hg^{2+} ions. Overall, these results confirmed that the sensitivity of the developed approach was found to detect beyond the maximum residue levels (MRLs) for Hg^{2+} in drinking water (2 ppb), as set by the Environmental Protection Agency[36] and the World Health Organization[37] and also below the estimated levels of Hg^{2+} found within shallow oceanic waters (~60–80 ppb).[38]

3.6 Selectivity of the SERS-sensor for Hg^{2+} detection

The selectivity of the AuNSt-PEG SERS-sensor was determined against thirteen additional metal ions (K^+, Zn^{2+}, Na^+, Mn^{2+}, Ag^+, Al^{3+}, Co^{2+}, Ca^{2+}, Fe^{2+}, Mg^{2+}, Bi^{3+}, Li^{4+}, Sn^{4+}) and a blank sample (AuNSt-PEG and dH_2O) (Fig. 5). These metal ions were introduced alone initially to ensure that the sensing mechanism was specific to Hg^{2+} detection. The results highlighted that Ag^+, Sn^{4+}, Co^{2+} and Fe^{2+} provided Raman enhancement in the presence of AuNSt-PEG and 1.25 mM TMB with 6% H_2O_2 (in comparison to the blank sample). All other metal ions alone remained similar to that of the blank. However, the only metal ion which significantly reduced the Raman enhancement (by ~80%) was Hg^{2+} ions. In additon, a mixture of all 13 metal ions without Hg^{2+} (Fig. 5, bar A) and 14 metal ions with Hg^{2+} (Fig. 5, bar B) were analysed and the results confirmed both an enhancment and reduction in SERS intensity from oxTMB, respectively. Therefore, this could confirm that the sensing mechanism was solely attributed to the presence of Hg^{2+} and the presence of other metal ions in a contaminated real water matrix would not have the same detrimental effect to the morphology of the AuNSt-PEG, as has been observed for Hg^{2+} ions.

3.7 Application and validation of the SERS-sensor in a seawater matrix

The applicability of the AuNSt-PEG SERS-sensor was analysed in two matrices: a certified coastal seawater Hg^{2+} certified reference material (CRM) and dH_2O conditions (Table 1). The results for AuNSt-PEG analysed in the CRM provided a working range between 0.1 ppb to 10^5 ppb (Fig. SI.13a†). A linear response between decreasing SERS intensity and increasing Hg^{2+} concentration, at a fixed Raman band of 1190 cm^{-1} was also observed (Fig. SI.13b†). Overall, the results showed good linearity for the seawater CRM (R^2 = 0.979) (Fig. SI.14†) and the lowest detectable limit of spiked Hg^{2+} ions was identified as 0.290 ppb, similar to that of the dH_2O conditions (LOD = 0.249 ppb). Therefore, the results suggest that the developed SERS-sensor could be applied to a real water sample, without suffering detrimentally from matrix effects. Finally, the assay CV (%) for all three water matrices fell below 7.2%, which was much lower than the

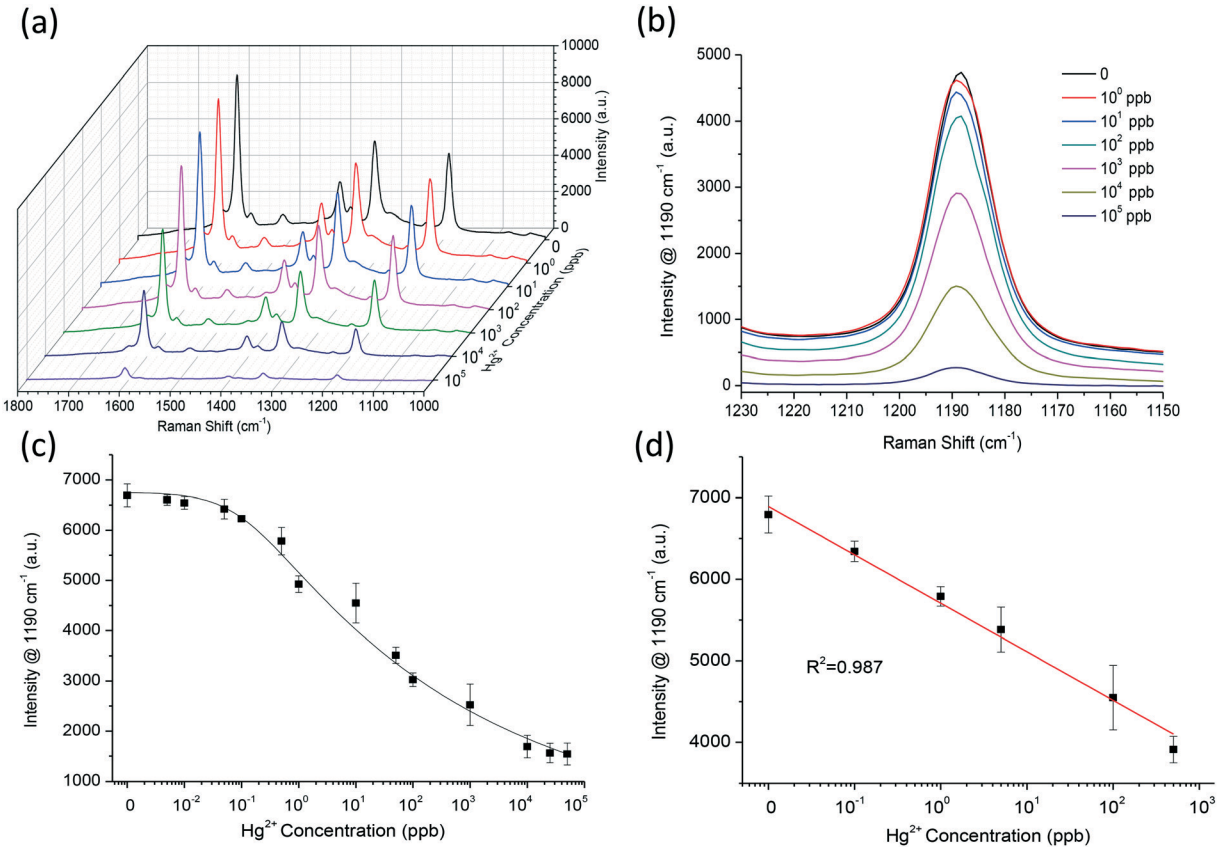

Fig. 4 Sensitivity of the SERS-sensor for detecting Hg^{2+} in dH_2O conditions. (a) Analysis of full Raman spectra illustrating three unique oxTMB peaks confirming that the Raman intensity is inversely proportional to Hg^{2+} concentration. (b) Analysis of oxTMB peak at 1190 cm^{-1} displaying the linear relationship between SERS intensity and Hg^{2+} concentration. (c) Calibration curve of AuNSt-PEG Raman intensity as a function of Hg^{2+} concentration. (d) Linear relationship between Hg^{2+} concentration and Raman intensity (R^2 = 0.987).

acceptable limit of 15%. The % recovery fell between the range of 95.2% and 104.5%, which overall confirmed the reliability and repeatability of the SERS-sensor. To provide a clearer picture of where the proposed system lies amongst other recent approaches reported in the literature for Hg^{2+} detection, several analytical parameters have been compared (Table 2). Although several rapid and sensitive detection mechanisms have been recently reported in the literature,[39–41] merits of the sensing approach presented in this study lie in its novel sensing mechanism, and that it was carefully validated for a real seawater matrix, which is a harsh environment for colloidal nanoparticles. Overall, it

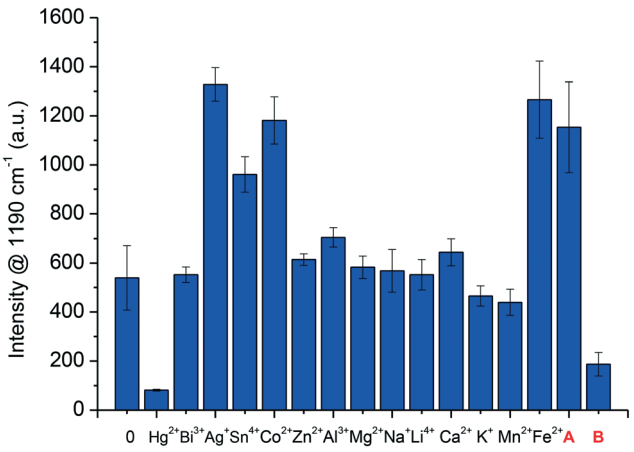

Fig. 5 Selectivity of the AuNSt-PEG Raman enhancement in the presence of additional individual metal ions all at 10 ppm and in the presence of a mix of 13 metal ions without Hg^{2+} (bar A) and 14 metal ions with Hg^{2+} (bar B), determined by analysing the oxTMB peak at 1190 cm^{-1}.

Table 1 Raman enhancement of AuNSt-PEG as a function of Hg^{2+} ion concentration after 20 min incubation with 1.25 mM TMB and 6% H_2O_2. The table compares the sensitivity and applicability of the assay in dH_2O conditions and a coastal Hg^{2+} seawater certified reference material (CRM). The table highlights the coefficient of variation (CV%) and % recovery to confirm reliability and repeatability of the approach. All validation was assessed in triplicate over three consecutive days (n = 27)

Matrix	LOD (ppb)	Spiked Hg^{2+} concentration (ppm)	CV (%)	Recovery (%)
dH_2O	0.249	0.001	3.4	99.3
		0.1	4.2	102.6
		10	2.7	98.4
Coastal Hg^{2+} seawater certified reference material (CRM)	0.290	0.001	7.2	97.1
		0.1	2.5	104.5
		10	6.6	95.2

Table 2 Comparison of analytical performance of the approach used in this work with several other systems reported in the literature for Hg^{2+} detection

Method	Matrix	Selectivity	Sensitivity	Validation	Recovery	Ref.
AuNSt: colorimetric (nanozyme) & SERS	Seawater CRM	Tested in presence of 13 other ions (K^+, Zn^{2+}, Na^+, Mn^{2+}, Ag^+, Al^{3+}, Co^{2+}, Ca^{2+}, Fe^{2+}, Mg^{2+}, Bi^{3+}, Li^{4+}, Sn^{4+})	0.2 ppb (1 nM)	Yes (CRM)	95.2–104.5%	This work
Bragg grating sensor	Drinking water	Tested in presence of 4 other ions (Pb^{2+}, Cu^{2+}, Na^+, Cd^{2+})	100 nM (20 ppb)	NA	86–98%	39
Conductometry	Tap, well and lake water	Tested in presence of 8 other ions (Na^+, Mg^{2+}, K^+, Ca^{2+}, Co^{3+}, Ni^{2+}, Cu^{2+}, Pb^{2+})	0.1 nM (0.02 ppb)	NA	NA	40
AuNPs: SERS	Drinking water	Tested in presence of 8 (Na^+, K^+, Mg^{2+}, Zn^{2+}, Cd^{2+}, Co^{2+}, Pb^{2+}, Cu^{2+})	60 aM (0.01 ppq)	Hg^{2+} concentrations validated against certified ICP-MS standards	NA	41
AuNPs: colorimetric (aggregation)	Deionised water, drinking water and seawater	Tested in presence of 19 other ions (Li^+, Na^+, K^+, Mg^{2+}, Ca^{2+}, Sr^{2+}, Ba^{2+}, Cr^{3+}, Mn^{2+}, Fe^{2+}, Fe^{3+}, Co^{2+}, Ni^{2+}, Cu^{2+}, Zn^{2+}, Cd^{2+}, Al^{3+}, Pb^{2+}, Ag^+)	100/200 nM (20/40 ppb)	NA	NA	42
Au–Cu nanobelt: SERS	Lake and tap water	Tested in presence of 7 other ions (K^+, Cu^{2+}, Fe^{3+}, Bi^+, Na^+, Cd^{2+}, Zn^{2+} and Cr^{3+})	8 ppt (5 pM)	NA	NA	43
AgNPs: colorimetric & SPR	Deionised water	Tested in presence of 11 other ions (Pb^{2+}, Cd^{2+}, Cu^{2+}, Co^{2+}, Ca^{2+}, Ni^{2+}, Zn^{2+}, Mn^{2+}, Fe^{2+}, Fe^{3+} and Na^+)	55 μM	NA	NA	44
AuNPs: colorimetric (nanozyme)	Lake water	Tested in presence of 14 other ions (Pb^{2+}, Na^+, K^+, Ca^{2+}, Mg^{2+}, Mn^{2+}, Fe^{2+}, Ni^{2+}, Sr^{2+}, Cu^{2+}, Zn^{2+}, Cd^{2+}, Al^{3+}, and Cr^{3+})	4 nM (0.8 ppb)	Yes	95–110%	45
AuNPs: colorimetric (aggregation)	Deionised water	Tested in presence of 13 other ions (Ti^{2+}, Mg^{2+}, V^{4+}, Mn^{2+}, Ni^{2+}, Cd^{2+}, Pb^{2+}, Cr^{2+}, Co^{2+}, Fe^{2+}, Zn^{2+}, Pt^{2+}, Ag^+)	10 pM (2 ppt)	NA	NA	46
PtNPs: colorimetric (nanozyme)	Grounds water	Tested in presence of 11 other ions (Li^+, Ca^{2+}, Al^{3+}, Cr^{3+}, Mn^{2+}, Co^{2+}, Ni^{2+}, Cu^{2+}, Zn^{2+}, Sn^{4+} and Pb^{2+})	47.3 nM (9.5 ppb)	NA	91.6–97.6%	47
AuNPs: colorimetric (aggregation)	Drinking water	Tested in presence of 17 other ions (Al^{3+}, Ba^{2+}, Ca^{2+}, Cd^{2+}, Co^{2+},Cr^{2+}, Cu^{2+}, Fe^{2+}, Fe^{3+}, Hg^{2+}, K^+, Mg^{2+}, Mn^{2+}, Na^+, Ni^{2+}, Pb^{2+} and Zn^{2+})	30 nM (6 ppb)	NA	NA	48
MoS_2 nanosheets: colorimetric (nanozyme)	Lake water	Tested in presence of 8 other ions (Ca^{2+}, Cd^{2+}, Mg^{2+}, Mn^{2+}, Ba^{2+}, Fe^{2+}, Cu^{2+} and Pb^{2+})	5 nM (1 ppb)	NA	93.9–98.9%	49
AgNPs: colorimetric (nanozyme) & SERS	Tap water	Tested in presence of 9 other ions (Ca^{2+}, Ba^{2+}, Pb^{2+}, Ni^{2+}, Sn^{2+}, Co^{2+}, Zn^{2+}, Mn^{2+} and Cd^{2+}). Two ions show some interference (Ag^+ and Cu^{2+})	1 nM (0.2 ppb)	NA	90–95%	11
Graphene oxide-PEI-Pd nanohybrids: colorimetric (nanozyme)	Wastewater	Tested in presence of 18 other ions (Na^+, K^+, NH_4^+, Ag^+, Ca^{2+}, Ba^{2+}, Cu^{2+}, Ni^{2+}, Zn^{2+}, Fe^{2+}, Mg^{2+}, Co^{2+}, Mn^{2+}, Cd^{2+}, Pb^{2+}, Al^{3+}, Fe^{3+} and Cr^{3+})	1 nM (0.2 ppb)	NA	NA	50

could be determined that in terms of sensitivity, selectivity and applicability our SERS approach provided an ultrasensitive sensing mechanism, with great potential for water and food safety applications.

4. Conclusion

In this study, we have successfully evaluated the catalytic performance and Raman scattering properties of the AuNSt coated with four different surface moieties (-NaCit/-PEG/-OEG/-11-MUA) based on their ability to produce oxTMB. AuNSt-PEG showed the best results as SERS substrates for oxTMB, therefore it was chosen for the detection of mercury ions in seawater. In the presence of Hg^{2+} ions, the catalytic activity of the AuNSt could be enhanced after Au–Hg amalgamation, evident by the production of a strong blue colour and absorption peaks at 370 nm and 650 nm, typical of oxTMB. As oxTMB is also highly Raman active, it would be reasonable to hypothesise that the Au–Hg amalgam would present a stronger Raman signal for oxTMB owing to the SERS effect of the AuNSt. However, experimental analysis interestingly showed a reduction in Raman intensity from the oxTMB reporter, in the presence of the AuNSt and Hg^{2+} ions, leading to a SERS signal which was inversely proportional to the Hg^{2+} concentration. Electron microscopy and elemental analysis further revealed that the presence of Hg^{2+} destructively truncated the sharp tips of the AuNSt changing their size, shape, and elemental composition. These findings provide important information about the peroxidase-mimicking and SERS properties of the AuNSt and the detrimental effect Au–Hg amalgam has on the morphology of AuNSt. Based on this mechanism, Hg^{2+} ion concentrations as

low as 0.2 ppb were successfully detected in both water and coastal seawater CRM samples. The approach also demonstrated high selectivity when tested against thirteen additional metal ions. Overall, the AuNSt-PEG provided an ultrasensitive and specific SERS-sensor for the detection of Hg^{2+} ions in high electrolyte environments. This research can contribute to the protection of water systems, aquatic life and human health from toxic Hg^{2+} contamination, with the potential for further developments to food matrices (*e.g.*, seafood) or on-site analysis in the future.

Author contributions

N. L., J. L, C. C. conceived the idea. N. L. characterized and validated the catalytic activity of AuNSt for the detection of Hg^{2+} ions. J. L. prepared and characterized the plasmonic and catalytic properties of AuNSt. C. E., C. C. acquired the funding and supervised the project. N. L., J. L., C. C. carried out data analysis and wrote the manuscript. All authors discussed the results, commented, reviewed, and edited the manuscript.

Conflicts of interest

The authors declare that they have no conflict of interest.

Acknowledgements

The authors J. L., C. E., C. C. acknowledge funding from the European Union's Horizon 2020 research and innovation program under the Marie Sklodowska-Curie Grant Agreement No. 720325. The author N. L. thanks the PhD studentship support from the Department of Employment and Learning for Northern Ireland (DEL).

References

1 T. W. Clarkson, The toxicology of mercury, *Crit. Rev. Clin. Lab. Sci.*, 1997, **34**(4), 369–403.
2 P. S. Islam, C. Chang, C. Selmi, E. Generali, A. Huntley, S. S. Teuber and M. E. Gershwin, Medical complications of tattoos: A comprehensive review, *Clin. Rev. Allergy Immunol.*, 2016, **50**(2), 273–286.
3 F. Beckers and J. Rinklebe, Cycling of mercury in the environment: Sources, fate, and human health implications: A review, *Crit. Rev. Environ. Sci. Technol.*, 2017, **47**(9), 693–794.
4 V. Kumar and B. Tate, Mercury, *J. Chem. Educ.*, 1982, **59**(11), 971–972.
5 R. Eisler, in *Mercury hazards to living organisms*, CRC Press, Boca Raton, Florida, USA, 1st edn, 2006, ch. 1, pp. 3–6.
6 N. Sui, F. Liu, K. Wang, F. Xie, L. Wang, J. Tang, M. Liu and W. W. Yu, Nano Au-Hg amalgam for Hg^{2+} and H_2O_2 detection, *Sens. Actuators, B*, 2017, **252**, 1010–1015.
7 G. L. Wang, X. F. Xu, L. H. Cao, C. H. He, Z. J. Li and C. Zhang, Mercury(ii)-stimulated oxidase mimetic activity of silver nanoparticles as a sensitive and selective mercury(ii) sensor, *RSC Adv.*, 2014, **4**(12), 5867–5872.
8 C. W. Tseng, H. Y. Chang, J. Y. Chang and C. C. Huang, Detection of mercury ions based on mercury-induced switching of enzyme-like activity of platinum/gold nanoparticles, *Nanoscale*, 2012, **4**(21), 6823–6830.
9 Z. Chen, C. Zhang, Q. Gao, G. Wang, L. Tan and Q. Liao, Colorimetric signal amplification assay for mercury ions based on the catalysis of gold amalgam, *Anal. Chem.*, 2015, **87**(21), 10963–10968.
10 L. Yan, Z. Chen, Z. Zhang, C. Qu, L. Chen and D. Shen, Fluorescent sensing of mercury(ii) based on formation of catalytic gold nanoparticles, *Analyst*, 2013, **138**(15), 4280–4283.
11 G. Qi, C. Fu, G. Chen, S. Xu and W. Xu, Highly sensitive SERS sensor for mercury ions based on the catalytic reaction of mercury ion decorated Ag nanoparticles, *RSC Adv.*, 2015, **5**(61), 49759–49764.
12 N. Logan, C. McVey, C. Elliott and C. Cao, Amalgamated gold-nanoalloys with enhanced catalytic activity for the detection of mercury ions (Hg^{2+}) in seawater samples, *Nano Res.*, 2020, **13**(4), 989–998.
13 M. Rex, F. E. Hernandez and A. D. Campiglia, Pushing the limits of mercury sensors with gold nanorods, *Anal. Chem.*, 2006, **78**(2), 445–451.
14 T. Senapati, D. Senapati, A. K. Singh, Z. Fan, R. Kanchanapally and P. C. Ray, Highly selective SERS probe for Hg(ii) detection using tryptophan-protected popcorn shaped gold nanoparticles, *Chem. Commun.*, 2011, **47**(37), 10326–10328.
15 S. Barbosa, A. Agrawal, L. Rodriguez-Lorenzo, I. Pastoriza-Santos, R. A. Alvarez-Puebla, A. Kornowski, H. Weller and L. M. Liz-Marzan, Tuning size and sensing properties in colloidal gold nanostars, *Langmuir*, 2010, **26**(18), 14943–14950.
16 S. K. Dondapati, T. K. Sau, C. Hrelescu, T. A. Klar, F. D. Stefani and J. Feldmann, Label-free biosensing based on single gold nanostars as plasmonic transducers, *ACS Nano*, 2010, **4**(11), 6318–6322.
17 E. Nalbant Esenturk and A. R. Hight Walker, Surface-enhanced raman scattering spectroscopy via gold nanostars, *J. Raman Spectrosc.*, 2009, **40**(1), 86–91.
18 W. Ma, M. Sun, L. Xu, L. Wang, H. Kuang and C. Xu, A SERS active gold nanostar dimer for mercury ion detection, *Chem. Commun.*, 2013, **49**(44), 4989–4991.
19 P. Zheng, M. Li, R. Jurevic, S. K. Cushing, Y. Liu and N. Wu, A gold nanohole array based surface-enhanced raman scattering biosensor for detection of silver(i) and mercury(ii) in human saliva, *Nanoscale*, 2015, **7**(25), 11005–11012.
20 Z. Yu, L. Chen, Y. Wang, X. Wang, W. Song, W. Ruan, B. Zhao and Q. Cong, A SERS-active enzymatic product used for the quantification of disease-related molecules, *J. Raman Spectrosc.*, 2014, **45**(1), 75–81.
21 K. S. McKeating, S. Sloan-Dennison, D. Graham and K. Faulds, An investigation into the simultaneous enzymatic and SERRS properties of silver nanoparticles, *Analyst*, 2013, **138**(21), 6347–6353.
22 S. Laing, A. Hernandez-Santana, J. Sassmannshausen, D. L. Asquith, I. B. McInnes, K. Faulds and D. Graham,

Quantitative detection of human tumor necrosis factor α by a resonance raman enzyme-linked immunosorbent assay, *Anal. Chem.*, 2011, **83**(1), 297–302.

23 C. Cao, L. C. Gontard, L. L. Thuy Tram, A. Wolff and D. D. Bang, Dual enlargement of gold nanoparticles: From mechanism to scanometric detection of pathogenic bacteria, *Small*, 2011, **7**(12), 1701–1708.

24 H. Yuan, C. G. Khoury, H. Hwang, C. M. Wilson, G. A. Grant and T. Vo-Dinh, Gold nanostars: Surfactant-free synthesis, 3D modelling, and two-photon photoluminescence imaging, *Nanotechnology*, 2012, **23**(7), 075102.

25 A. B. Serrano-Montes, D. Jimenez de Aberasturi, J. Langer, J. J. Giner-Casares, L. Scarabelli, A. Herrero and L. M. Liz-Marzán, A general method for solvent exchange of plasmonic nanoparticles and self-assembly into SERS-active monolayers, *Langmuir*, 2015, **31**(33), 9205–9213.

26 E. M. Hotze, T. Phenrat and G. V. Lowry, Nanoparticle aggregation: Challenges to understanding transport and reactivity in the environment, *J. Environ. Qual.*, 2010, **39**(6), 1909–1924.

27 J. Lou-Franco, B. Das, C. Elliott and C. Cao, Gold nanozymes: From concept to biomedical applications, *Nano-Micro Lett.*, 2020, **13**(1), 10.

28 J. C. Love, L. A. Estroff, J. K. Kriebel, R. G. Nuzzo and G. M. Whitesides, Self-assembled monolayers of thiolates on metals as a form of nanotechnology, *Chem. Rev.*, 2005, **105**(4), 1103–1170.

29 C. G. Khoury and T. Vo-Dinh, Gold nanostars for surface-enhanced raman scattering: Synthesis, characterization and optimization, *J. Phys. Chem. C*, 2008, **112**(48), 18849–18859.

30 C. Muehlethaler, K. Ng, L. Gueissaz, M. Leona and J. R. Lombardi, Raman and SERS characterisation of solvent dyes: An example of shoe polish analysis, *Dyes Pigm.*, 2017, **137**, 539–552.

31 E. C. Le Ru, E. Blackie, M. Meyer and P. G. Etchegoin, Surface enhanced raman scattering enhancement factors: A comprehensive study, *J. Phys. Chem. C*, 2007, **111**(37), 13794–13803.

32 Q. Su, X. Ma, J. Dong, C. Jiang and W. Qian, A reproducible SERS substrate based on electrostatically assisted APTES-functionalized surface-assembly of gold nanostars, *ACS Appl. Mater. Interfaces*, 2011, **3**(6), 1873–1879.

33 C. Hrelescu, T. K. Sau, A. L. Rogach, F. Jäckel, G. Laurent, L. Douillard and F. Charra, Selective excitation of individual plasmonic hotspots at the tips of single gold nanostars, *Nano Lett.*, 2011, **11**(2), 402–407.

34 B. Pelaz, P. del Pino, P. Maffre, R. Hartmann, M. Gallego, S. Rivera-Fernandez, J. M. de la Fuente, G. U. Nienhaus and W. J. Parak, Surface functionalization of nanoparticles with polyethylene glycol: Effects on protein adsorption and cellular uptake, *ACS Nano*, 2015, **9**(7), 6996–7008.

35 Y. J. Long, Y. F. Li, Y. Liu, J. J. Zheng, J. Tang and C. Z. Huang, Visual observation of the mercury-stimulated peroxidase mimetic activity of gold nanoparticles, *Chem. Commun.*, 2011, **47**(43), 11939–11941.

36 Environmental Protection Agency (EPA), Ground water and drinking water fact sheet: mercury [online], 2016, https://archive.epa.gov/water/archive/web/pdf/archived-technical-fact-sheet-on-mercury.pdf (accessed June 2021).

37 World Health Organisation (WHO), *Guidelines for Drinking-water quality* 3rd edition, Geneva, World Health Organization [online], 2004, https://www.who.int/water_sanitation_health/dwq/GDWQ2004web.pdf (accessed June 2021).

38 C. H. Lamborg, C. R. Hammerschmidt, K. L. Bowman, G. J. Swarr, K. M. Munson, D. C. Ohnemus, P. J. Lam, L. E. Heimbürger, M. J. A. Rijkenberg and M. A. Saito, A global ocean inventory of anthropogenic mercury based on water column measurements, *Nature*, 2014, **512**(7512), 65–68.

39 B. S. Kavitha, S. Sridevi, P. Makam, D. Ghosh, T. Govindaraju, S. Asokan and A. K. Sood, Highly sensitive and Rapid detection of mercury in water using functionalized etched fiber Bragg grating sensors, *Sens. Actuators, B*, 2021, **333**, 129550.

40 M. Pandeeswar, S. P. Senanayak and T. Govindaraju, Nanoarchitectonics of small molecule and DNA for ultrasensitive detection of mercury, *ACS Appl. Mater. Interfaces*, 2016, **8**, 30362–30371.

41 P. Makam, R. Shilpa, A. E. Kandjani, S. R. Periasamy, Y. M. Sabri, C. Madhu, S. K. Bhargava and T. Govindaraju, SERS and fluorescence-based ultrasensitive detection of mercury in water, *Biosens. Bioelectron.*, 2018, **100**, 556–564.

42 C. Y. Lin, C. J. Yu, Y. H. Lin and W. L. Tseng, Colorimetric sensing of silver(I) and mercury(II) ions based on an assembly of Tween 20-stabilized gold nanoparticles, *Anal. Chem.*, 2010, **82**, 6830–6837.

43 H. Bao, H. Fu, L. Zhou, W. Cai and H. Zhang, Rapid and ultrasensitive surface-enhanced Raman spectroscopy detection of mercury ions with gold film supported organometallic nanobelts, *Nanotechnology*, 2020, **31**, 155501.

44 S. Manivannan and R. Ramaraj, Silver nanoparticles embedded in cyclodextrin–silicate composite and their applications in Hg(ii) ion and nitrobenzene sensing, *Analyst*, 2013, **138**, 1733–1739.

45 C.-I. Wang, C.-C. Huang, Y.-W. Lin, W.-T. Chen and H.-T. Chang, Catalytic gold nanoparticles for fluorescent detection of mercury(II) and lead(II) ions, *Anal. Chim. Acta*, 2012, **745**, 124–130.

46 M. P. Cecchini, V. A. Turek, A. Demetriadou, G. Britovsek, T. Welton, A. A. Kornyshev, J. D. E. T. Wilton-Ely and J. B. Edel, Heavy metal sensing using self-assembled nanoparticles at a liquid–liquid interface, *Adv. Opt. Mater.*, 2014, **2**, 966–977.

47 A. J. Kora and L. Rastogi, Peroxidase activity of biogenic platinum nanoparticles: A colorimetric probe towards selective detection of mercuric ions in water samples, *Sens. Actuators, B*, 2018, **254**, 690–700.

48 D. Liu, W. Qu, W. Chen, W. Zhang, Z. Wang and X. Jiang, Highly sensitive, colorimetric detection of mercury(II) in aqueous media by quaternary ammonium group-capped

gold nanoparticles at room temperature, *Anal. Chem.*, 2010, **82**, 9606–9610.

49 S. Kavitha, S. M. J. Kala and A. A. B. Christus, Colorimetric detection of Hg (II) sensor based on MoS2 nanosheets acting as peroxidase mimics, *Orient. J. Chem.*, 2021, **37**(3), 679–682.

50 S. Zhang, D. Zhang, X. Zhang, D. Shang, Z. Xue, D. Shan and X. Lu, Ultratrace naked-eye colorimetric detection of Hg^{2+} in wastewater and serum utilizing mercury-stimulated peroxidase mimetic activity of reduced graphene oxide-PEI-Pd nanohybrids, *Anal. Chem.*, 2017, **89**, 3538–3544.